ARTICLES

Front Propagation in Patterned Precipitation. 2. Electric Effects in Precipitation−Dissolution Patterning Schemes

M. Al-Ghoul[†,‡] and R. Sultan*[,†]

Department of Chemistry and Center for Advanced Mathematical Sciences, American University of Beirut, Beirut, Lebanon

Received: November 13, 2002

In this paper, we continue the simulation of periodic precipitation systems with redissolution using the model of Müller and Polezhaev (MP). In the first paper of this sequence (*J. Phys. Chem. A* **2001**, *105*, 8053), we proposed a reaction scheme involving precipitation and redissolution to which the MP model was adapted. Maps of Liesegang bands and diffusion profiles were calculated at different concentrations of the inner and outer electrolytes. In this paper, we extend the study to the investigation of the effect of an applied constant electric field on the front propagation. Two reaction schemes, representative of the $Co(OH)_2$ and $Cr(OH)_3$ precipitation/redissolution systems, are studied. In the former scheme, the band stratum propagates faster, and the spacing between the bands increases with increasing field strength, exactly reproducing the experimental behavior. In the latter, treated under conditions yielding a single propagating band, two opposing trends are observed: at high field, the propagation is slower at higher field strength, whereas at sufficiently low field, the propagation is enhanced with increasing field strength. Wave stopping occurs at the location reached at the same time in a field-free experiment. This results in the field-on curve crossing the field-free curve at the stopping time, just resembling the experimental observation. Other interesting patterning properties are reported and discussed.

1. Introduction

In a previous paper,[1] we presented a model to simulate the propagation of a $Co(OH)_2$ Liesegang[2,3] pattern (from Co^{2+} and NH_4OH) in a gelled medium. Such a system displays a stratum of parallel bands that propagates because of band formation due to precipitation at the bottom and band disappearance by dissolution at the top. $Co(OH)_2$ dissolves in excess NH_4OH because of the formation of the complex ion $Co(NH_3)_6^{2+}$.[4] The whole set of bands thus migrates down a vertical tube.[5] Other Liesegang systems with redissolution such as HgI_2[6] and $Cr(OH)_3$[7] were also studied and reported in the literature.

Because ionic species are involved in the system of diffusion and chemical reactions underlying the dynamics of the propagation, an electric field applied across the reaction−diffusion medium is expected to exhibit a significant effect on the properties of the pattern. Das et al. studied the effect of a constant electric field on a propagating single HgI_2 band in one[8] and two[9] dimensions. The behavior of other Liesegang systems in an electric field was also investigated, notably the $Co(OH)_2$ in 1D[10] and the $Cr(OH)_3$ in 2D.[11] Interesting effects such as the acceleration of the propagation in the presence of the field,[8−11] a reversal of the trend with varying concentration of the inner electrolyte across a characteristic time,[10] and wave stopping and annihilation[11] are observed. Lagzi[12] presented a model based on that of Büki,[13] incorporating the electric field term in a two-variable reaction−diffusion scheme involving a single precipitation reaction. The model captures some of the observed features—mainly the effect of field strength on the spacing ratio in both positive and negative fields. We focus here on two systems considered in previous experimental studies involving redissolution in excess diffusing electrolyte, namely, the $Co(OH)_2$ (from Co^{2+} and NH_4OH) and $Cr(OH)_3$ (from Cr^{3+} and NaOH) systems. The chemical processes involved in each system are as follows:

(1) $Co(OH)_2$:

$$Co^{2+}(aq) + 2NH_4OH(aq) \rightarrow 2NH_4^{+}(aq) + Co(OH)_2(s) \quad (1)$$

$$Co(OH)_2(s) + 6NH_4^{+}(aq) \rightarrow Co(NH_3)_6^{2+}(aq) + 2H_2O(l) + 4H^{+}(aq) \quad (2)$$

(2) $Cr(OH)_3$:

$$Cr^{3+}(aq) + OH^{-}(aq) \rightarrow Cr(OH)_3(s) \quad (3)$$

$$Cr(OH)_3(s) + OH^{-}(aq) \rightarrow Cr(OH)_4^{-}(aq) \quad (4)$$

* Corresponding author. E-mail: rsultan@aub.edu.lb.
† Department of Chemistry.
‡ Center for Advanced Mathematical Sciences.

10.1021/jp022433p CCC: $25.00
Published on Web 01/31/2003

The above schemes are reduced to simpler ones for analysis using the model of Polezhaev and Müller,[1,14] as explained in the next section.

2. Model and Equations

We now present the simplified reaction schemes, followed by the reaction−diffusion equations describing the dynamics, now augmented by the electric field interaction term for the charged species.

2.1. Co^{2+}/NH_4OH System. We introduce the following variables:

$$X = Co^{2+}(aq)$$
$$Y = NH_4OH(aq)$$
$$Z = NH_4^{+}(aq)$$
$$A = Co(OH)_2(s)$$

The $Co(OH)_2$ reaction scheme is reduced to a simpler form[1] as follows:

$$X + 2Y \xrightarrow{k} 2Z + A \tag{5}$$

$$A + 6Z \xrightarrow{k'} P \tag{6}$$

We assume that the dissolved salt of concentration c is different from the complex $Co(NH_3)_6^{2+}(aq)$, called P in eq 6. The conservation equations for the concentrations of the various species diffusing and reacting are given by

$$\frac{\partial X}{\partial t} = D_X \frac{\partial^2 X}{\partial \xi^2} - kXY^2 - \epsilon_x \frac{\partial X}{\partial \xi} \tag{7}$$

$$\frac{\partial Y}{\partial t} = D_Y \frac{\partial^2 Y}{\partial \xi^2} - 2kXY^2 \tag{8}$$

where D_X and D_Y are diffusion coefficients of X and Y, respectively; ξ is a 1D spatial variable; k is a precipitation rate constant; $\epsilon_x = 2u_xE$, where u_x is the mobility of ion X; and E is the electric field strength. The addition of excess Z induces the dissolution of the precipitate in the form of the complex $Co(NH_3)_6^{2+}(aq)$. The evolution of Z is given by

$$\frac{\partial Z}{\partial t} = D_Z \frac{\partial^2 Z}{\partial \xi^2} - 6k'Z^6\rho + 2kXY^2 - \epsilon_z \frac{\partial Z}{\partial \xi} \tag{9}$$

where D_Z is the diffusion coefficient of species Z and k' denotes the rate constant of dissolution; $\epsilon_z = u_zE$ (note here that $z_x = +2$, $z_y = 0$, and $z_z = +1$ from the defining expressions of X, Y, and Z).

Let $\tilde{\rho}$ denote the average density of solid salt in the form of small particles (called nuclei in ref 14), and ρ, the average density of solid salt in the form of big particles. The dynamics of the average particle sizes, $\tilde{\rho}$ and ρ for precipitate A, is given by

$$\frac{\partial \tilde{\rho}}{\partial t} = \upsilon_1(c) - [\upsilon_2(c) + \upsilon_3(c)]\tilde{\rho} \tag{10}$$

$$\frac{\partial \rho}{\partial t} = \upsilon_3(c)\tilde{\rho} + \upsilon_4(c)\rho - 6k'Z^6\rho \tag{11}$$

The concentration of dissolved salt, c, is given by

$$\frac{\partial c}{\partial t} = D_c \frac{\partial^2 c}{\partial \xi^2} + kXY^2 - \upsilon_1(c) + \upsilon_2(c)\tilde{\rho} - \upsilon_4(c)\rho + 6k'Z^6\rho \tag{12}$$

where D_c is the diffusion coefficient of dissolved salt.

The rate functions $\upsilon_i(c)$ are taken to be simple monotonic functions of c as follows:

$$\upsilon_1(c) = \alpha(c - c_3)\,\theta(c - c_3) \tag{13}$$

$$\upsilon_2(c) = \beta(c_2 - c)\,\theta(c_2 - c) \tag{14}$$

$$\upsilon_3(c) = \gamma(c - c_2)\,\theta(c - c_2) \tag{15}$$

$$\upsilon_4(c) = \delta(c - c_1)\,\theta(c - c_1) \tag{16}$$

where α, β, γ, and δ are rate constants and $\theta(x)$ is the Heaviside function. Here, $\upsilon_1 \equiv$ rate of nucleation as c exceeds some critical value c_3; $\upsilon_3 \equiv$ rate of transition of nuclei into big particles as c exceeds some other parameter c_2. If c_2 is not exceeded, then the nuclei dissolve at a rate υ_2. Finally, $\upsilon_4 \equiv$ rate of growth of large particles as c exceeds a certain value c_1. It is shown[14] that the explicit form of the $\upsilon_i(c)$'s does not affect the qualitative behavior of the result. We assume that the effect of the electric field on the dissolved salt P will not affect the dynamics of X, Y, and Z; no reaction-diffusion equation for P is written.

2.2. Cr^{3+}/NaOH System. For the $Cr(OH)_3$ system, we now define the following variables:

$$W = Cr^{3+}(aq)$$
$$Y = OH^{-}(aq)$$
$$Q = Cr(OH)_4^{-}(aq)$$
$$B = Cr(OH)_3(s)$$

The reaction scheme for $Cr(OH)_3$ (eqs 3 and 4) is reduced to a simpler form as follows:

$$W + 3Y \xrightarrow{k} B \tag{17}$$

$$B + Y \xrightarrow{k'} Q \tag{18}$$

We assume that the dissolved salt of concentration c is different from the complex $Cr(OH)_4^{-}(aq)$, called Q in eq 18. The evolution equations for the concentrations of the species involved in the above scheme are given by

$$\frac{\partial W}{\partial t} = D_W \frac{\partial^2 W}{\partial \xi^2} - kWY^3 - \epsilon_w \frac{\partial W}{\partial \xi} \tag{19}$$

$$\frac{\partial Y}{\partial t} = D_Y \frac{\partial^2 Y}{\partial \xi^2} - 3kWY^3 - k'Y\rho + \epsilon_y \frac{\partial Y}{\partial \xi} \tag{20}$$

where D_W and D_Y are diffusion coefficients of W and Y, respectively; k is a precipitation rate constant; and $\epsilon_w = 3u_wE$ and $\epsilon_y = u_yE$ (since $z_x = +3$ and $z_y = -1$).

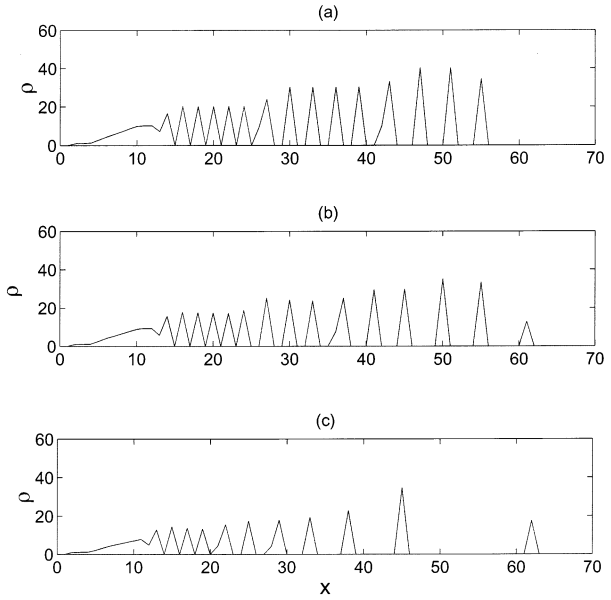

Figure 1. Pattern of $Co(OH)_2$ (*A*) precipitate bands (plotted as ρ versus x) at a fixed time $t = 38 \times 10^5$ and a varying electric field strength. Model parameters: $X_0 = 10$; $Y_0 = 400$; $Z_0 = 0$; $\tilde{\rho}_0 = 0$; $\rho_0 = 0$; $k = 1.0 \times 10^{-5}$; $k' = 1.0 \times 10^{-4}$; $D_X = D_Y = D_c = 1.0 \times 10^{-5}$; $D_Z = 1.0 \times 10^{-2}$; $c_1 = 2.1$; $c_2 = c_3 = 3.0$; $\alpha = 0.02$; $\beta = 0.01$; $\gamma = 0.01$; $\delta = 0.002$. (a) $\epsilon_x = 0.0$; $\epsilon_y = 0.0$ (field-free). (b) $\epsilon_x = 1.0 \times 10^{-6}$; $\epsilon_y = 5.0 \times 10^{-7}$. (c) $\epsilon_x = 3.0 \times 10^{-6}$; $\epsilon_y = 1.5 \times 10^{-6}$ (3 times the previous field strength).

The dynamics of the average particle sizes, $\tilde{\rho}$ and ρ for precipitate *B*, is here given by

$$\frac{\partial \tilde{\rho}}{\partial t} = v_1(c) - [v_2(c) + v_3(c)]\tilde{\rho} \tag{21}$$

$$\frac{\partial \rho}{\partial t} = v_3(c)\tilde{\rho} + v_4(c)\rho - k'Y\rho \tag{22}$$

The concentration of dissolved salt, c, is given by

$$\frac{\partial c}{\partial t} = D_c \frac{\partial^2 c}{\partial \xi^2} + kXY^3 - v_1(c) + v_2(c)\tilde{\rho} - v_4(c)\rho + k'Y\rho \tag{23}$$

where D_c is the diffusion coefficient of dissolved salt.

The rate functions $v_i(c)$ are the same as those in eqs 13−16. We assume that the effect of the electric field on the dissolved salt Q will not affect the dynamics of W and Y; no reaction−diffusion equation for Q is written. Because, experimentally, we obtain one band instead of a stratum in the $Cr(OH)_3$ case, we work within the framework of conditions that is known to yield this result, thus taking $c_1 > c_2 = c_3$. It was established[1] that this condition (which reverses the one imposed in section 2.1, see the caption of Figure 1) constitutes a criterion for the transition to the single-band propagation regime.

2.3. Numerical Solution. The reaction−diffusion equations for the Co^{2+} and Cr^{3+} systems were solved numerically with the following initial conditions

$$X(t = 0, x) = X_0\theta(x - L/2)$$

$$Y(t = 0, x) = Y_0\theta(L/2 - x)$$

$$\tilde{\rho}(t = 0, x) = \rho(t = 0, x) = Z(t = 0, x) = c(t = 0, x) = 0$$

and the following no-flux boundary conditions

$$\mathbf{n}\cdot\nabla X|_{x=L} = \mathbf{n}\cdot\nabla Y|_{x=L} = \mathbf{n}\cdot\nabla Z|_{x=L} = \mathbf{n}\cdot\nabla c|_{x=L} = 0$$

where x is the spatial independent variable (denoted ξ in the reaction-diffusion equations) and L is the length of the tube in which the reaction is taking place. The length L is partitioned into an equally spaced mesh of 400 grid points. L is taken to be 100; therefore, the grid size $\delta = 0.25$. The partial differential equations are then discretized according to a second-order centered finite difference scheme to compute the 1D Laplacians

$$\nabla^2 f = \frac{\partial^2 f}{\partial \xi^2} = \frac{f_{j+1} - 2f_j + f_{j-1}}{\delta^2} \tag{24}$$

and the advective terms due to the electric field that consist of a first-order derivative (here in 1D) are discretized according to the following up-wind scheme:

$$\nabla f = \frac{\partial f}{\partial \xi} = \frac{f_{j+1} - f_j}{\delta} \tag{25}$$

The resulting ordinary differential equations are very stiff and thus solved using Gear's method[15] for stiff differential equations. We decreased the size of the mesh by increasing the number of grid points to 800, keeping the same length. The results did not change qualitatively. The number of bands and the spacing remained the same.

3. Results and Discussion

3.1. Co^{2+}/NH_4OH System. Equations 7−12 were solved numerically as described in section 2.3. The function $\rho(t)$ yields the spatial distribution of the precipitate pattern. The time evolution of $\rho(t)$ in an electric field-free system was given in Figure 1 of ref 1. It shows the band formation at the front of the pattern and the band disappearance (by dissolution) at the tail as time advances. Figure 1 here shows $\rho(t)$ at a specific time but at various field strengths. As expected, the pattern migrates further in space at a higher field strength, as indicated by the location of both the last and the first bands. Furthermore, the band spacing increases with field strength (see notably the spacing between the last two bands and its variation in frames a through c), capturing the effect seen in Figure 5 of ref 10. Figure 2 shows the corresponding diffusion curves (calculated as the distance of last band d_{lb} versus time t). We clearly see that the higher-field curves lie above the lower-field ones, consistent with the conjecture in Figure 1 and in conformity with the results of Sultan and Halabieh.[10]

We now turn our attention to the effect of varying the concentration of the inner electrolyte ($Co^{2+} \equiv X_0$) at constant field strength. Figure 3 displays four frames showing a high concentration curve (dashed line) and the variation of concentration below that high value, in a gradual increase from a to d, indicated by the solid curve. The trend in the four lower concentrations is a gradual increase in the velocity of propagation as X_0 increases, thus exactly reversing the field-free trend wherein the pattern propagates faster in a less concentrated X domain. This is illustrated by the position of the solid curve, which is higher up as X_0 is increased. However, an interesting situation occurs with the high-concentration extreme. We see that as we go from frames a to c the solid curve lies below the dashed curve, then crosses the latter, and then moves above it, revealing the competition between the electric field factor and the X concentration factor as X_0 increases to high values. Note that the crossing obtained in frame b captures the features

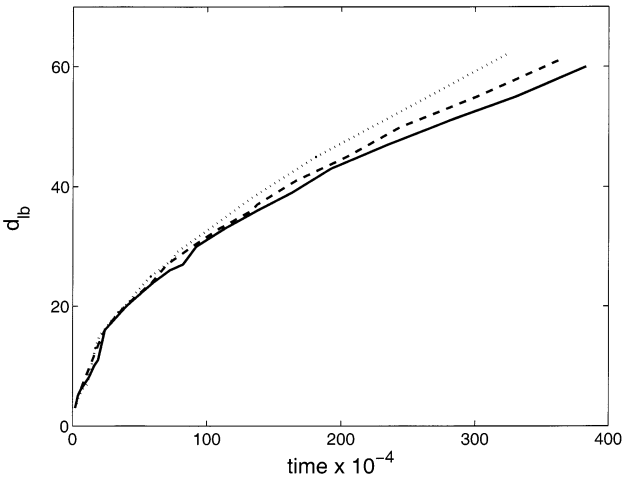

Figure 2. Diffusion profiles (calculated as the distance of the last band d_{lb} versus time t) for the A precipitate propagation at different electric field strengths corresponding to the patterns of Figure 1. (—): Field-free; (− −): $\epsilon_x = 1.0 \times 10^{-6}$, $\epsilon_y = 5.0 \times 10^{-7}$; (· ·): $\epsilon_x = 3.0 \times 10^{-6}$, $\epsilon_y = 1.5 \times 10^{-6}$ (3 times the previous field strength).

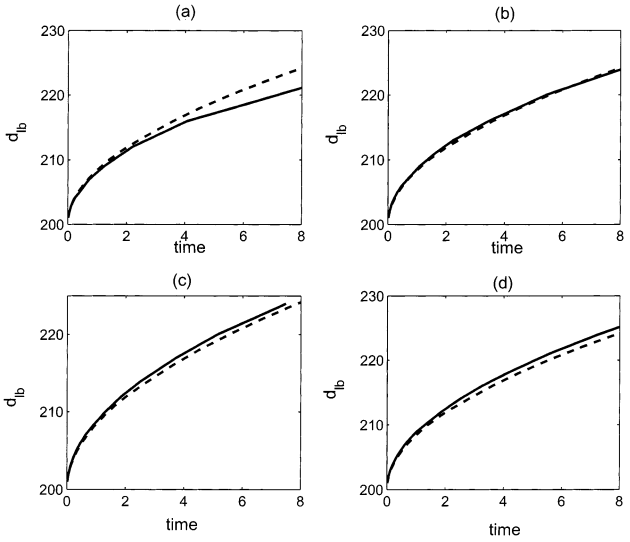

Figure 3. Diffusion profiles (d_{lb} versus time t) at a fixed electric field strength, $\epsilon_x = 1.0 \times 10^{-6}$; $\epsilon_y = 5.0 \times 10^{-7}$ but with a varying concentration of inner electrolyte X_0. In all of the frames, (− −) $X_0 = 13.0$. (—): (a) $X_0 = 5.0$, (b) $X_0 = 6.0$, (c) $X_0 = 6.5$, (d) $X_0 = 8.5$.

observed in the experiments of ref 10, where a critical time (the time of the crossing) marks the transition between the two opposite trends. In the latter work, however, all of the curves intersect nearly at the same point, revealing a more concerted and systematic behavior than what is obtained from the calculations. The most interesting feature here remains that it is at high concentration that the field-free trend is restored, namely, that the propagation becomes hindered if the X concentration is high enough to dominate the effect of the electric field (frames c and d). The crossing between many curves at the same point observed experimentally[10] could be obtained by appropriately adjusting the initial concentration of the diffusing reagent Y (NH_4OH) and the electric field strength E. This was not attempted here.

3.2. Cr^{3+}/NaOH System. The numerical solution of eqs 19−23 was performed in a manner similar to the one in the last section but in the single-band regime (see the end of section 2.2). Figure 4a shows diffusion curves (calculated as the distance between the interface and the leading edge of the single band, d, versus time t). The solid line represents the field-free curve.

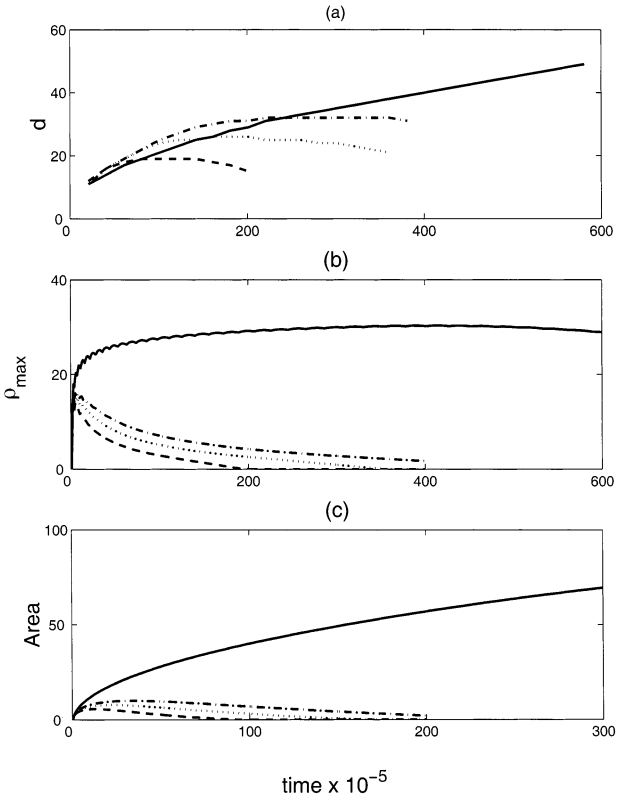

Figure 4. (a) Diffusion curves (d vesus t) for the B precipitate at high electric field strengths. The trend is that a propagating ring is slowed as the electric field strength increases. (—): $\epsilon_w = 0.0$, $\epsilon_y = 0.0$; (− −): $\epsilon_w = 2 \times 10^{-6}$, $\epsilon_y = 4.0 \times 10^{-7}$; (· ·): $\epsilon_w = 1.5 \times 10^{-6}$, $\epsilon_y = 3.0 \times 10^{-7}$; (− · −): $\epsilon_w = 1.2 \times 10^{-6}$, $\epsilon_y = 2.4 \times 10^{-7}$. The plateau regions start right at the field-free curve, indicating a constant location/wave-stopping phenomenon (they can be rubbed out). (b) Plot of the maximum of density ρ_{max} versus time t. (c) Plot of the area under the $\rho - x$ pulse versus time t. The pulse gradually disappears as the field strength increases (same curve designation as in plot a). Model parameters: $X_0 = 10$; $Y_0 = 50$; $Z_0 = 0$; $\tilde{\rho}_0 = 0$; $\rho_0 = 0$; $k = 1.0 \times 10^{-5}$; $k' = 1.0 \times 10^{-4}$; $D_X = D_Y = D_c = 1.0 \times 10^{-5}$; $D_Z = 1.0 \times 10^{-2}$; $c_1 = 3.0$; $c_2 = c_3 = 2.1$; $\alpha = 0.02$; $\beta = 0.01$; $\gamma = 0.01$; $\delta = 0.002$.

The other curves are obtained with the field on, at three different strengths. The first interesting observation is that all three curves reach a plateau as the field-free curve is crossed. This reproduces the experimental behavior obtained in 2D,[11] namely, the so-called wave-stopping phenomenon. When the ring reaches a position attained in the same time lapse during a field-free experiment, it is slowest there, with zero velocity. The plateau regions were omitted in the figure of ref 11. The calculated trend (obtained in Figure 4a) is that the lower field strength curves lie above the higher field ones (i.e., that the band travels faster at lower field strengths). This opposes the trend obtained experimentally in 2D, and thus, the problem warrants an exploration of a wider range of field strengths (discussed below). At this stage, it may appear strange that the zero field strength curve lies below all of the other curves, although the trend is that the latter go higher up as the field strength *decreases*. This is understood on the basis that as the field strength decreases the curves move higher up but flatten and thus tend to the field-free curve. This effect is proved using a scaling argument developed in the Appendix. Figure 4b and c displays the time evolution of the maximum density ρ_{max} and the area under the $\rho - x$ profile, respectively. Both quantities decrease as the field strength increases at a given time, apparently marking the importance of dissolution as the field is turned on (the curves

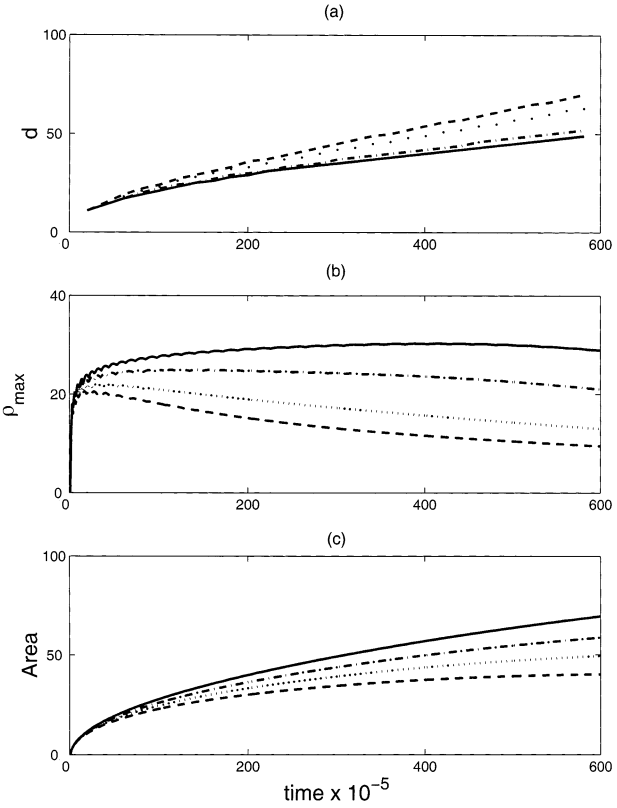

Figure 5. (a) Diffusion curves (d vesus t) for the B precipitate at low electric field strengths. The trend here is that propagation is enhanced as the electric field strength increases (just the opposite of the previous case). (—): $\epsilon_w = 0.0$, $\epsilon_y = 0.0$; (− −) : $\epsilon_w = 6.0 \times 10^{-7}$; $\epsilon_y = 1.2 \times 10^{-7}$; (• •): $\epsilon_w = 3.0 \times 10^{-7}$; $\epsilon_y = 6.0 \times 10^{-8}$; (− • −): $\epsilon_w = 2 \times 10^{-7}$, $\epsilon_y = 4.0 \times 10^{-8}$. (b) Plot of the maximum of density ρ_{max} versus time t. (c) Plot of the area under the $\rho - x$ pulse versus time t. Here, the pulse becomes thicker as time advances, but its thickness shrinks as the field strength increases at a fixed time.

are located significantly below the field-free one) and its growing role as the field strength increases (curves are further below with increasing field strength).

We now explore a wider range of field strengths. Interestingly, we find that at sufficiently low field strengths the trend in the diffusion curves matches the one observed experimentally in 2D $Cr(OH)_3$ systems, as clearly seen in Figure 5a. This reversal of behavior is a particularly interesting result that is reminiscent of the general properties of chemical wave−electric field interactions. A reversal in the direction of wave propagation was conjectured in the presence of a constant electric field as a critical time is crossed[16] or as the field strength increases through a critical value.[17] To our knowledge, a reversal in speed variation with increasing field strength was observed experimentally only when accompanied by wave splitting[18,19] or when the electric field changes sign.[18,20] In theoretical studies, opposite variations in the speed of propagation with field strength are due to the multiple valuedness of the solutions.[16,21,22] Thus, these two opposite trends (at high and low field values) warrant further investigation. Though not explored experimentally in the work of Sultan and Panjarian,[11] a link can be established between this conjectured reversal in trend and the observed ring annihilation at high field.[11] The opposing trend at high field could perhaps be a transition toward the gradual decrease in the velocity of propagation until complete annihilation is reached, the latter represented by the disapperance of the $d - t$ curve (Figure 4a).

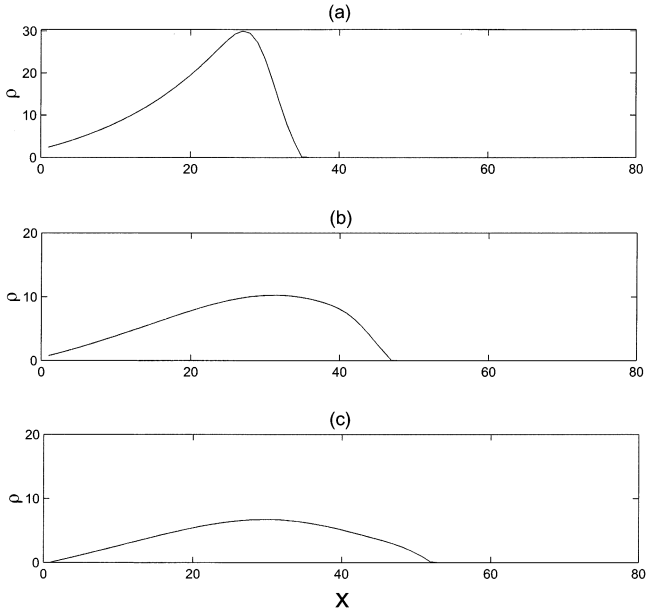

Figure 6. Pulse profile of precipitate B for the low-field case and its time evolution. In frames a−c, we vary the field strength. (a) $\epsilon_w = 0.0$, $\epsilon_y = 0.0$. (b) $\epsilon_w = 2 \times 10^{-7}$, $\epsilon_y = 4.0 \times 10^{-8}$. (c) $\epsilon_w = 6.0 \times 10^{-7}$, $\epsilon_y = 1.2 \times 10^{-7}$; $t = 4 \times 10^6$. The pulse propagates faster as the field strength increases.

The trends in ρ_{max} and the area are preserved at low field (see Figure 5b and c) with one notable difference, namely, that the area increases with time (instead of vanishing), just like the field-free case. This feature also captures the experimental observation whereby the ring becomes thicker as time advances. Finally, a very interesting feature is noticed in the ρ_{max} versus time field-free curve, namely, the oscillations detected notably at early times (Figure 5b). Such oscillations, not apparent in the experimental results of ref 11, suggest a very interesting experiment to investigate this behavior. The anticipated $\rho - x$ profile would then be a breathing pulse in the vertical direction because the density maximum exhibits an undulatory time evolution. The electric field contribution seems to tame such oscillations.

Figure 6 shows the time evolution of a B precipitate pulse profile (ρ versus x) and its variation with field strength in the low-field regime (domain of Figure 5). It is clearly seen that the pulse migrates further (at a given time t) as the field strength increases, reproducing the experimental results.[11] The oscillations in the field-free case, detected in Figure 5b, are not discerned in Figure 6, as a highly time-resolved evolution is required.

4. Conclusions

The above study reveals a rich dynamics that yields diverse behavior and a wealth of variety in structure. Many experimental features could be accounted for, and the model even suggested new behavior that has so far remained unexplored. This encompasses mainly the low-field versus high-field behavior and the ρ_{max} oscillations in the field-free case, both obtained in the $Cr(OH)_3$ single-band propagation. Therefore, interesting new experiments are suggested.

The model of Müller and Polezhaev is one of the few models with a kind of a comprehensive nature. It incorporates the diffusion, nucleation, dissolution, and kinetics of particle growth in a simplified scheme. The present treatment adds to it the possibility of postprecipitation redissolution. Some limitations in the theory include neglecting the mechanism of stepwise

aggregation and fragmentation of the Becker-Döring type,[24] the role of the precipitate particle size distribution (PSD),[23] and the effect of the electric field on the precipitate density. An oscillating electric field causes unstable ions to precipitate at nucleation sites having an electrical charge. Precipitate nuclei and crystals thus grow, affecting the values of $\tilde{\rho}$ and ρ. In the case of a constant electric field (such as the one applied here), this effect is neglible with respect to ion−ion interaction in solution. Note that the determination of the precipitate surface charge density itself generally depends on knowledge of the PSD.[25] The modeling of growth and coarsening could be subjected to a more rigorous treatment.[26] Yet, despite its simple kinetic formulation, the model captures complex spatial structures such as helecoidal structures,[14,27] dislocations, and "Saturn rings"[14] in addition to the classical 1D parallel Liesegang bands and 2D concentric rings.

The main findings of the present study may now be summarized as follows:

• **Modeling $Co(OH)_2$ Bands Propagation:** Charged species Co^{2+} and NH_4^+; see eqs 1 and 2; the charged product species $Co(NH_3)_6^{2+}$ and H^+ do not enter into the kinetics.

(1) The pattern of $Co(OH)_2$ bands propagates faster in the electric field. The velocity of propagation and the band spacing increase with increasing field strength.

(2) When the concentration of inner electrolyte (X_0) is varied, two opposing trends in the relative positions of the diffusion curves exist, bridged by a situation where two curves at different concentrations intersect. In the latter event, the opposing trends exist before and after the crossing time.

• **Modeling $Cr(OH)_3$ Single Band Propagation:** Charged species Cr^{3+} and OH^-; see eqs 3 and 4; the charged product species $Cr(OH)_4^-$ does not affect the kinetics. The simulations are performed in the regime where a single band is obtained (see ref 1).

(1) At high field, the propagation is slower with increasing field strength. The propagation stops at the crossing point with the field-free curve.

(2) At sufficiently low field, the propagation is enhanced with increasing field strength.

(3) Dissolution, marked by the decrease in the band maximum density, is enhanced by the electric field at long times.

(4) The simulations predict time oscillations in the peak of precipitate density notably in the field-free case. This characteristic, not accounted for previously, was recently verified by the experiments of Hilal and Sultan.[28]

Acknowledgment. This work was supported by a University Research Board (URB) grant, American University of Beirut.

Appendix: High-Field and Low-Field Behavior

It is known that for Liesegang patterns, in the absence of an applied external electric field, the dynamics of a traveling band exhibits a Fickian profile (i.e., the distance traveled $d \approx t^{1/2}$, where t is time). In general, we can write this as

$$d = A_0 t^{1/2} + C_0 \tag{26}$$

where A_0 is a positive constant and C_0 is another real constant.

Recent experiments by Sultan et al.[10,11] on Liesegang band propagation in the presence of an electric field show that the above law can be modified as

$$d = A(\epsilon) t^{1/2} + B(\epsilon) t + C(\epsilon) \tag{27}$$

where ϵ is the strength of the applied electric field and $A(\epsilon)$, $B(\epsilon)$, and $C(\epsilon)$ are parameters depending on ϵ. These parameters must satisfy the following constraints:

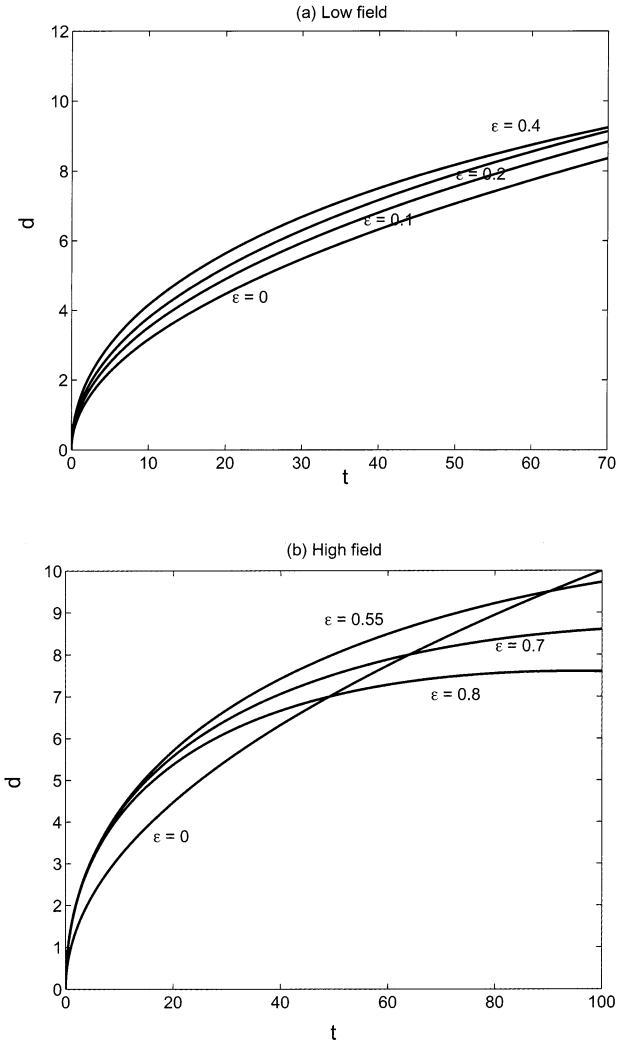

Figure 7. Behavior in the low-field (a) and high-field (b) regimes for the propagating $Cr(OH)_3$ pulse according to the scaling model discussed in the Appendix (eqs 27−32). $\epsilon_0 = 0.5$, $A_0 = 1$, and $C_0 = 1$. At $\epsilon < \epsilon_0$ (low field), the trend is like that in Figure 5a. As ϵ increases through ϵ_0, the trend is reversed, yielding the behavior seen in Figure 4a. In both cases, the curves tend toward the zero-field curve as $\epsilon \rightarrow 0$.

$$A(\epsilon = 0) = A_0 \tag{28}$$

$$B(\epsilon = 0) = 0 \tag{29}$$

$$C(\epsilon = 0) = C_0 \tag{30}$$

To recover and understand the switch in the trend of the diffusion profiles between the low-field and high-field cases, there must be definite criteria for the dependence of the parameters $A(\epsilon)$ and $B(\epsilon)$ on ϵ. We can deduce from the numerical simulations that in the case of low field strength (i.e., when ϵ is less than a certain threshold ϵ_0) $A(\epsilon)$ is an increasing function of ϵ. As ϵ increases through ϵ_0, $A(\epsilon)$ shall be a decreasing function of ϵ. The simplest model is when A is a quadratic function of the field strength as follows:

$$A(\epsilon) = A_0(1 + \epsilon) + \epsilon(\epsilon_0 - \epsilon) \tag{31}$$

In addition, $B(\epsilon)$ is always a decreasing function of the field strength ϵ. The simplest form is the following linear decrease:

$$B(\epsilon) = -\epsilon \tag{32}$$

One can easily verify that in the limit of $\epsilon \rightarrow 0$ A and B will smoothly tend to A_0 and 0, respectively. The threshold field strength ϵ_0 is the value at which the trend in the diffusion profiles is reversed. At field strengths of $\epsilon < \epsilon_0$, A increases with ϵ. When ϵ crosses ϵ_0, A starts decreasing with ϵ, giving rise to the effect exhibited in Figure 4a.

As an example, by letting the threshold field strength $\epsilon_0 = 0.5$, $A_0 = 1$, and $C_0 = 1$, we obtain the plots shown in Figure 7, which qualitatively explain the simulation results in the presence of an electric field in the high- and low-field regimes. It is interesting to see that in both situations the curves tend toward the zero-field curve as $\epsilon \rightarrow 0$.

References and Notes

(1) Al-Ghoul, M.; Sultan, R. *J. Phys. Chem. A* **2001**, *105*, 8053.

(2) Liesegang, R. E. *Lieseg. Phot. Archiv.* **1896**, *21*, 221. Liesegang, R. E. *Naturewiss. Wochenschr.* **1896**, *11*, 353.

(3) Henisch, H. K. *Crystals in Gels and Liesegang Rings*; Cambridge University Press: Cambridge, U.K., 1988.

(4) Lloyd, F. E.; Moravek, V. *Plant Physiol.* **1928**, *3*, 101.

(5) Nasreddine, V.; Sultan, R. *J. Phys. Chem. A* **1999**, *103*, 2934.

(6) Das, I.; Pushkarna, A.; Argawal, N. R. *J. Phys. Chem.* **1989**, *93*, 7269.

(7) Zrınyi, M.; Gálfi, L.; Smidróczki, É.; Rácz, Z.; Horkay, F. *J. Phys. Chem.* **1991**, *95*, 1618.

(8) Das, I.; Pushkarna, A.; Bhattacharjee, A. *J. Phys. Chem.* **1990**, *94*, 8968.

(9) Das, I.; Pushkarna, A.; Bhattacharjee, A. *J. Phys. Chem.* **1991**, *95*, 3866.

(10) Sultan R.; Halabieh, R. *Chem. Phys. Lett.* **2000**, *332*, 331.

(11) Sultan, R.; Panjarian, Sh. *Physica D* **2001**, *157*, 241.

(12) Lagzi, I. *Phys. Chem. Chem. Phys.* **2002**, *4*, 1268.

(13) Büki, A.; Kárpáti-Smidróczki, E.; Zrinyi, M. *J. Chem. Phys.* **1995**, *103*, 10387.

(14) Müller, S. C.; Polezhaev, A. A. *Chaos* **1994**, *4*, 631.

(15) Kahaner, D.; Moler, C.; Nash, S. *Numerical Methods and Software;* Prentice Hall: Englewood Cliffs, NJ, 1989.

(16) Ševčiková, H.; Marek, M. *Physica D* **1986**, *21*, 61.

(17) Schmidt, S.; Ortoleva, P. *J. Chem. Phys.* **1979**, *71*, 1010.

(18) Ševčiková, H.; Marek, M. *Physica D* **1984**, *13*, 379.

(19) Feeney, R.; Schmidt, S. L.; Ortoleva, P. *Physica D* **1981**, *2*, 536.

(20) Ševčiková, H.; Marek, M. *Physica D* **1983**, *9*, 140.

(21) Ortoleva, P. *Physica D* **1987**, *26*, 67.

(22) Sultan, R. F. *Chem. Phys. Lett.* **1997**, *266*, 145.

(23) Ozkan, G.; Ortoleva, P. *J. Chem. Phys.* **2000**, *112*, 10510.

(24) Wattis, J. A. D. *J. Phys. A: Math. Gen.* **1999**, *32*, 8755.

(25) Seaver, A. E. In *Magnetic Helicity in Space and Laboratory Plasmas*; Brown, M. R., Canfield, R. C., Pevtsov, A., Eds.; Geophysical Monographs; American Geophysical Union: Washington, DC, 1999; Vol. 111.

(26) Ratke, L.; Vorhees, P. W. *Growth and Coarsening: Ostwald Ripening in Material Processing*; Springer: Berlin, 2002.

(27) Chernavskii, D. S.; Polezhaev, A. A.; Müller, S. C. *Physica D* **1991**, *54*, 160.

(28) Hilal, N.; Sultan R., submitted to *Chem. Phys. Lett.*